

High-resolution single-shot phase shifting interference microscopy using deep neural network

Sunil Bhatt, ^{a)} Ankit Butola, ^{a)} Sheetal Raosaheb Kanade, Anand Kumar, and Dalip Singh Mehta ^{b)}

Bio-photonics and Green Photonics Laboratory, Department of Physics, Indian Institute of Technology Delhi, Hauz-Khas, New Delhi 110016, India

White light phase shifting interference (WL-PSI) microscopy is a prominent technique for high-resolution quantitative phase imaging (QPI) of industrial and biological specimens. Highly sensitive and accurate phase measurement is possible using WL-PSI because of low coherence properties of light source and the phase shifting algorithm. Multiple phase-shifted interferograms with accurate phase shift is obligatory in WL-PSI for measuring accurate phase map of the object. However, phase error occurs during the experimentation due to environmental perturbation and recording multiple frames. Here, we present a single-shot phase shifting interferometric technique for accurate phase measurement using filtered WL-PSI and deep neural network (DNN). The method is implemented by training the DNN to generate the phase shifted frames from a single recorded interferogram that are equivalent to experimentally recorded phase shifted interferograms. We simulate and experimentally demonstrate the robustness of the proposed framework on strip step-like waveguide structure. The results show precise matching of reconstructed phase map from the DNN generated phase shifted interferograms and experimentally recorded interferograms. The current WL-PSI+DNN approach may further strengthen QPI techniques by high resolution phase recovery using single frame for different biomedical applications.

Quantitative phase imaging (QPI) is a rapidly emerging label free technique to reconstruct quantitative information related to the refractive index and local thickness of the specimens.¹ Ultra-portable QPI instruments have been developed as an add-on module with a standard microscope to acquire multi-modal information of the object.²⁻⁴ The experimental and computational advancement in QPI is being widely adopted for extracting quantitative information about various industrial and biological applications such as human red blood cells (RBC), tissue sections, and sperm samples, among others.⁵⁻⁹ Various newly developed QPI techniques have been implemented which mainly focuses on to improve the resolution, temporal phase sensitivity, acquisition rate and spatial phase sensitivity of the system.¹ In QPI system, the spatial phase sensitivity and data acquisition rate are inversely related to each other. For example, coherent light, i.e., laser-based QPI techniques offer single-shot recording and phase reconstruction of the specimens due to high spatial and temporal coherent nature of the laser source. Though, fast data acquisition rate in coherent QPI technique is very popular for live cell imaging but the presence of speckle noise degrades the spatial phase sensitivity hence unable to offer the phase map of thin biological specimens.⁵

Phase-shifting white light interference microscopy (PS-WLIM) is the most commonly used technique for sub-nanometric highly sensitive for height measurement in both industrial and biological specimens.¹⁰⁻¹³ Further, the use of low coherent light source such as halogen

lamp and light emitting diode (LED) causes no speckle noise and without spurious fringes thus improves the spatial phase sensitivity of the system, significantly. In WLIM, reference and sample beams are equally displaced to obtain the phase information of the object, encoded in the form of spatially modulated signal. Equal displacement of reference and sample arms results low fringe density in the interferogram hence direct Fourier transform (FT) phase retrieval technique cannot be used.¹⁴ The implementation of FT algorithm requires high density interference fringes to separate the DC and twin image term for noise free phase recovery. To accomplish this sufficiently large tilt angle is introduced between the reference and object beams, thus essentially making it off-axis interferometry. Under these conditions, high fringe density throughout the field of view cannot be achieved using white light source, due to its low spatial and temporal coherence. Therefore, on-axis optical geometry and recording of multiple phase shifted interferograms i.e., phase shifting interferometry (PSI) is essential for phase recovery in low coherence interferometry at full detector resolution. Significant amount of work has been done in the development of various PSI technique for various applications.^{15,16} In PSI, a pre calibrated piezoelectric transducer (PZT) and sufficient time requisite to record precise phase-shifted multiple interferograms quickly. However, the requirement of multiple frames is the key obstacle in PSI for many applications such as live cell imaging and measurement with dynamic samples. Therefore, various single-shot phase-shifting approaches have been

^{a)} Contributed equally to this work.

^{b)} Corresponding Author: mehtads@physics.iitd.ac.in

developed in the past.¹⁷⁻¹⁹ These approaches suffer with complex experimental setups while using multiple CCD camera, and significantly increases the cost of the system. Other, approached such as using polarizer array for phase shifting purpose leads inefficient utilization of the CCD chip.¹⁹

Here, we propose a single-shot phase shifting interference microscopy (SS-PSIM) with filtered white light source to achieve high resolution phase imaging using deep neural network (DNN). The method is implemented by capturing five phase shifted frames with the low coherent source and a compact interferometric objective lens. Further, generative adversarial network (GAN) is trained to generate later four phase shifted frames from the first interferometric frame. After sufficient training, the line profile of the network generated images further compared with the experimentally recorded datasets. Further, performance of the network is evaluated by comparing the phase maps reconstructed from the generated interferograms and the ground truth (experimentally recorded) interferograms. Our simulation and experimental results on rib waveguide shows the potential of the proposed framework for single-shot high resolution phase imaging of step like industrial object. The data driven approach for high resolution QPI is useful for the biological application especially in live cell imaging.

The idea behind the phase shifting interferometry is to introduce systematic phase shifts between reference and sample fields such that the intensity equation becomes:²⁰

$$I(x, y) = I_s(x, y) + I_r(x, y) + 2\sqrt{I_s(x, y)I_r(x, y)} \cos[\phi(x, y) + \delta(t)] \quad (1)$$

where $\delta(t)$ is the controlled phase shift added purposely between reference and sample field. Different phase shifting techniques have been proposed in the past to extract the phase $\phi(x, y)$ of the object. Out of which, five phase shifted interferometry is preferred because of moderate phase error and acquisition time.²⁰ The phase information $\phi(x, y)$ of the object can be calculated from the following expression:²⁰

$$\phi(x, y) = \tan^{-1} \left[\frac{2(I_4(x, y) - I_2(x, y))}{I_1(x, y) - 2I_3(x, y) + I_5(x, y)} \right] \quad (2)$$

Though the phase shifting interferometry offers high spatial resolution but less preferred because of slow acquisition rate and thus cannot be applicable for live cells imaging. Therefore, we used generative adversarial network (GAN) based deep neural network (DNN) framework to predict the phase shifted frames i.e., $I_2(x, y), I_3(x, y), I_4(x, y)$ and $I_5(x, y)$ from the first $I_1(x, y)$ interferogram.

GAN comprised of simultaneous training of two models generator (G) and discriminator (D).^{21,22} The generator model takes an image as an input dataset and generates some mapped image. The discriminator differentiates between two inputs target image (ground truth) and generated image (output of generator). Discriminator further calculated the losses and gives feedback to generator for fine tuning. The GAN architecture developed in the present study is shown in Fig. 1. The modified U-net consisted encoder and decoder blocks where each block in the encoder is comprised of convolution layer, batch norm, and Leaky rectifier linear unit (ReLU) as an activation function.²³ Also, each block of decoder comprised of transposed convolution layer, batch norm, dropout, and a ReLU activation function.²³ There are also skip connections between encoder and decoder as in any U-net. The generator architecture is shown in Fig. 1 takes interferogram as an input, and after successive iterations, it predicts phase shifted interferogram images with minimum loss.

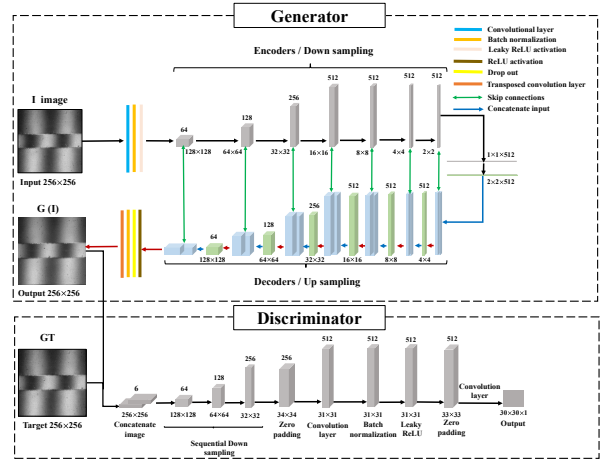


FIG. 1. Generative adversarial network (GAN) architecture for single shot high resolution quantitative phase imaging using phase shifting interference microscopy.

The architecture of the discriminator is a PatchGAN.^{23,24} Number of blocks in the discriminator model depicts in Fig. 1. Each block in discriminator is composed of convolution layer, batch norm, and Leaky ReLU as an activation function.²³ The shape of the output after the last layer is a batch size of $30 \times 30 \times 1$. Each 30×30 patch of the output classifies a 70×70 portion of the input image.²³ Initially, the 'I image' is given as input to the untrained generator model as shown in Fig. 1. The generated image G (I) and the ground truth (GT) is then fed into the discriminator again shown in Fig .1. Further the calculated losses based on the outputs of generator G (I) and discriminator are given as a feedback for fine-tuning until the losses

are minimum. The discriminator loss (l_{disc}) calculated using sigmoid cross entropy as a function of discriminator outputs, $D(GT)$ and $D(G(I))$. The discriminator loss function is defined by²⁴

$$l_{disc} = -(\log D(GT) + (\log(1 - D(G(I)))) \quad (3)$$

The generated loss (l_{gen}) is the sum of sigmoid cross entropy - a function of $D(G(I))$ and scaled mean absolute error (MAE) between real image and the generated image. It is given by the equation²⁴:

$$l_{gen} = -(\log D(G(I)) + \alpha |GT - G(I)|) \quad (4)$$

Here, the parameter α was set as 100 as optimized value after multiple trials. After calculating the losses, the trainable parameters were updated using an adaptive moment estimation (Adam) optimizer with a learning rate 2×10^{-4} for both generator and discriminator networks. The random normal initializer was used to initiate the convolution layers in first down sampling and up sampling blocks. The truncated normal distribution was used to initialize weights while zero initializer was adopted for the network bias terms. The model first trained and optimized on the simulated waveguide objects and further on the experimental

datasets. Google colab is used for the training and testing of the network. The dataset divided (simulated as well as experimental) into two parts: training ($\sim 80\%$) and test dataset ($\sim 20\%$). For training, first interferogram was taken as an input of the network and figure out the losses i.e., generator loss and discriminator loss.²¹⁻²⁴ These losses are then feedback to the corresponding networks until the discriminator achieve the equal probability (i.e., $\sim 1/2$) of getting target and generated image.²¹

Figure 2 shows the comparison between reconstructed phase map from simulated interferograms and GAN generated phase shifted interferograms. Five phase shifted interferograms are simulated on a waveguide like structure. The large dataset is simulated by varying fringe density, width and height of the step object. Total 300 set of phase shifted interferograms with equal phase shifting are simulated in the present study. Out of 300, 80% of the datasets are used to train the network and 20% is used for testing purpose with 61 epochs in the network. The batch size of 1, input image size 256×256 ²³ and the buffer size of 400 was used during the training of the network. In our case the training time required for training of network is $\sim 4-5$ hrs.

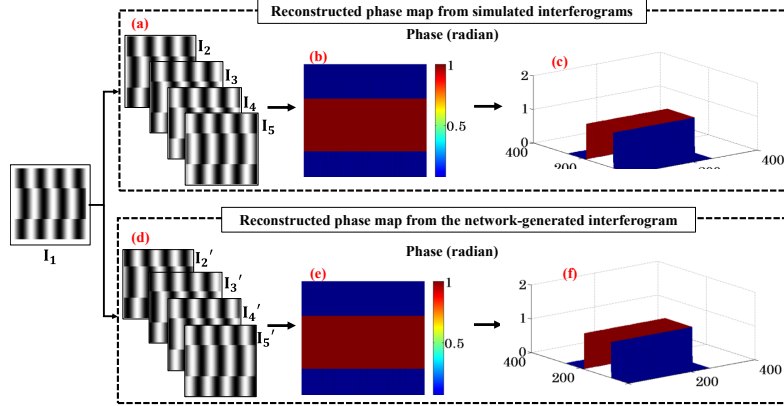


FIG. 2. Comparison between the simulated and network generated five phase shifted interferograms. (a) Simulated five equally phase-shifted interferograms. (b) and (c) are their corresponding 2D, and 3D reconstructed phase-map using five-step phase-shifting algorithm, respectively. (d) Network (GAN) generated four equally phase-shifted interferograms for same input interferogram I_1 . (e) and (f) are their corresponding 2D, and 3D reconstructed phase-map, respectively

The training process started by taking first interferogram (I_1) as an input of the generator, which generates four equal phase-shifted interferogram. The generated output are compared with the simulated interferogram (I_1, I_2, I_3, I_4 and I_5) to minimize the loss and to update the trainable parameters. The final trained network is selected to predict the phase shifted frames (I_2', I_3', I_4' and I_5') from the single interferogram i.e. I_1 as shown in Fig. 2. The simulated and generated

interferograms are further analyzed by using Eq. 2 to obtain the phase map of the object. The reconstructed phase map from the simulated and predicted interferograms is shown in Fig. 2 (b) and (e), respectively. Moreover, Fig. 2 (c) and (f) shows 3D phase map of the object reconstructed from simulated and predicted interferograms, respectively. We observe that the peak-to-valley phase error between Fig. 2 (c) and (f) are found to be ± 20 mrad. Some modulation in

the network generated phase map occurred due to slight mismatching of the equal phase shifts between the generated interferograms. Since it has been shown in the previous study that the mismatch between the phase shift $\delta(t)$ as shown in Eq. 1 is proportional to the background modulation in the reconstructed phase map.²⁵ In our case, the modulation is very less hence might be a very small mismatch between the phase shifts $\delta(t)$ of the generated interferograms. The proposed framework further realized experimentally by using filtered white light phase shifted interference microscopy system.

The experimental setup of white light phase shifted interference microscopy (WL-PSIM) to realize single shot high-resolution QPI is shown in Fig. 3. The working principle of WL-PSIM is based on the principle of white light interference microscopy. In this system, the divergent light from the halogen (12V50W, LV-LH50PC) lamp as a white light source is passes through a narrow band pass green filter of 520 nm peak wavelength with ± 40 nm bandwidth. Thus, the light emerges from the band pass filter lay in the wavelength range of green light (520 nm) of visible spectra (400-700 nm). Lens L_1 collected the emergent filtered light and focus it on the aperture stop (A-stop). The aperture stop controls the spatial coherence of light source by varying the size of aperture. Further, lens L_2 collects all converging light from output of A-stop, and collimated for the uniform illumination at the sample plane. The field-stop (F-stop) controls the field of view (FOV) of the objective lens. The beam-splitter BS_1 directs the light towards the sample plan through the Mirau-objective lens (Nikon, CF Plan, 50X/0.55DI, and WD 3.4).

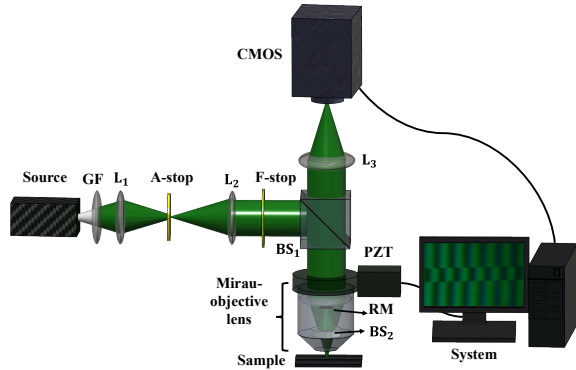


FIG. 3. The schematic diagram of filtered white light phase-shifting interference microscope (F-WL-PSIM). GF: green-filter, L_1 , L_2 and L_3 : lenses, A-stop: aperture-stop, F-stop: field-stop, BS_1 and BS_2 : beam splitter, PZT: piezo-electric transducer, RM: reference mirror, CMOS: complementary metal-oxide-semiconductor.

The Mirau objective lens is comprised of a reference mirror (RM) at the back aperture and a beam splitter BS_2 in the front plane of the lens. The BS_2 reflect light towards the RM and transmit light towards the sample.

The Mirau-objective lens is attached with the piezo-electric transducer (NV40 3CLE), which generate equal temporal phase-shifted data frames. The back-reflected light from the sample interferes with reflected light from RM at BS_2 which further focused by the lens L_3 at CCD camera (INFINITY2-1C). The captured phase-shifted interferograms are further used for phase reconstruction of the specimen using the 5-step phase-shifting algorithm.

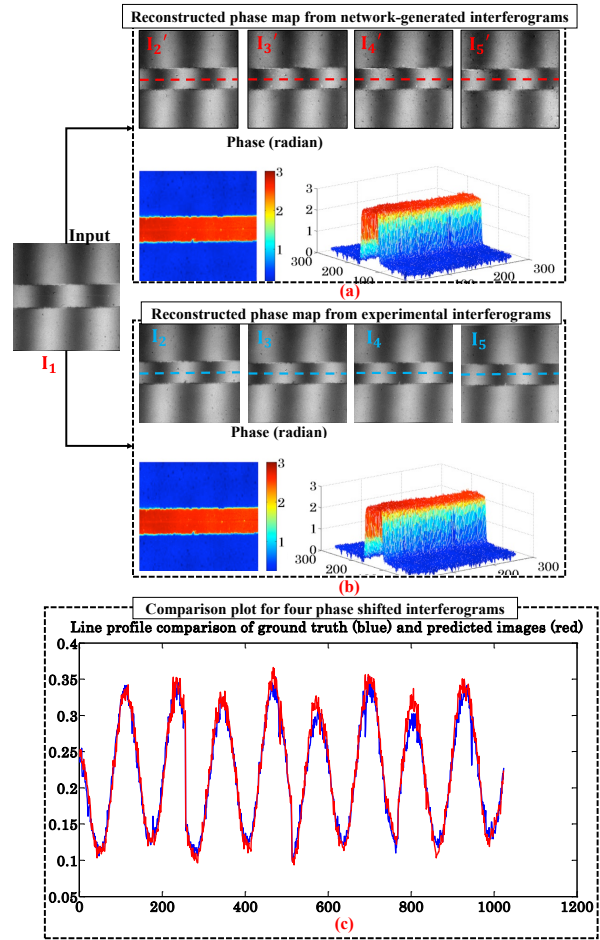


FIG. 4. Comparison between the reconstructed phase maps from network generated interferogram and experimentally recorded interferogram on waveguide structure. (a) The network generated equal phase-shifted interferograms, and their corresponding 2D and 3D reconstructed phase-map using five-step phase-shifted algorithm. (b) Experimentally captured five phase-shifted interferograms along with I_1 assisted with PZT and their corresponding 2D and 3D reconstructed phase-map using five-step phase-shifted algorithm. (c) Line profile comparison plot of equal four phase-shifted interferogram (with an image size of (0,256) each) for network predicted after training (red) and experimentally captured through the setup (blue).

Figure 4 shows the comparison between the reconstructed phase maps from network generated interferograms and experimentally recorded interferograms. The experiment is performed on the

strip waveguide structure. The waveguide was taken as a standard sample to compare between reconstructed phase map from network generated i.e. (I_2', I_3', I_4' and I_5') and experimentally recorded interferogram i.e. (I_1, I_2, I_3, I_4 and I_5). The network was trained on the first interferogram i.e. I_1 to predict the four equally phase shifted frames.

To perform the training and testing of the network, total 270 sets of phase-shifted interferograms were recorded by using PS-WLIM system. Total 236 sets (~80% of total datasets) were used to train the network and 34 sets for the testing purpose for the training of the network with 21 epochs in the network. Other parameter such as input image size of 256×256 , the buffer size of 400 and training time ~ 4-5 hrs were used during the training of the network similar as simulation part. After sufficient training of network, it provides us single-shot equally phase-shifted interferograms within the time limit of < 1 second. Figure 4 (a) are the results from the network generated interferograms obtained from the trained network and its corresponding phase-map. Figure 4 (b) are the results obtained from the multi-shot PSI assisted with well calibrated PZT interferogram captured in F-WL-PSIM setup and their corresponding reconstruction of the optical waveguide. We got similar results with the experimental dataset (i.e. waveguide object) as that we got for the simulated datasets (i.e. step-like object).

Further, to validate the results achieved with trained network generated interferograms and the interferograms captured experimentally, we performed the line profile measurement along the center line of the interferograms, as shown in Fig. 4 (a) and (b). The comparative results are shown in Fig. 4 (c) that the blue and red plot are the line profile of four phase-shifted interferograms assisted with experimental captured (ground truth) and network generated (predicted) interferograms along the center line respectively. Figure 4 (c) shows the corresponding image size of the network generated and experimental captured four phase shifted interferograms along the common x-axis respectively. Along the x-axis, first (0, 256) interval is corresponds to first phase shifted interferogram line profile comparison of network generated and experimental captured interferogram, second (256, 512) and so on. Figure 4 (c) depicted the comparison plot got the best result with overlapping of line profile for the network generated (red) and experimentally taken (blue) four phase-shifted interferograms. Thus, the line profile comparison validates the better performance of our trained network.

In our approach, using WL-PSIM+DNN once the network is trained for a given set of data, it provides us the multiple equally phase-shifted interferograms for a single input. Thus, this approach is single-shot and less time consuming as compare to the other phase-shifting approach.

In conclusion, we have demonstrated a WL-PSIM + DNN framework for single-shot high-resolution phase imaging purpose. WL-PSIM offers highly sensitive measurements of industrial and biological object by utilizing full resolution of the system. However, multiple phase-shifted frames are required for the phase reconstruction in PSI²⁶ thus cannot be applicable for biological applications such as live cell imaging. In this study, deep learning architecture i.e. GAN is utilized to perform single-shot QPI using WL-PSIM. The current framework first simulated on step like object and further experimentally shown on a step like waveguide structure. The line profile of network generated interferograms plotted against the experimentally recorded frames to check accuracy of the architecture. The network generated and experimentally recorded interferograms are further used to reconstruct the phase map of the object using standard phase shifting algorithm. In our data-set acquisition, we required 30 seconds of time for capturing one set of five phase shifted data frames through a pre-calibrated WL-PSIM. But after sufficient training of DNN, network provide us the same dataset of equally phase-shifted interferograms within the time limit of < 1 second. Thus, using our approach, we reduce the time consumption during pre-calibration of PZT and the experimental capturing of one phase shifted dataset \gg 30 times. Thus, we provide approx. 30 times better performance in time management using WL-PSIM+DNN compare to pre-calibrated WL-PSIM. The data driven approach will be useful for single-shot high resolution phase imaging for other industrial and biological specimen. The proposed method is useful for the QPI of biological cells and tissues such as human RBCs, and cancer tissues where high resolution phase imaging is important in disease diagnosis and identification of cancer margin. The data are available upon reasonable request.

- 1 G. Popescu, *Quantitative Phase Imaging of Cells and Tissues*. (McGraw-Hill Education, 2011).
- 2 Y. Jo, S. Park, J. Jung, J. Yoon, H. Joo, M. H. Kim, S. J. Kang, M. C. Choi, S. Y. Lee, and Y. Park, *Science advances* **3** (8), e1700606 (2017).
- 3 Gabriel Popescu, Takahiro Ikeda, Ramachandra R. Dasari, and Michael S. Feld, *Opt. Lett.* **31** (6), 775 (2006).
- 4 Amardeep S. G. Singh, Arun Anand, Rainer A. Leitgeb, and Bahram Javidi, *Opt. Express* **20** (21), 23617 (2012).
- 5 Ankit Butola, Daria Popova, Dilip K Prasad, Azeem Ahmad, Anwarul Habib, Jean Claude Tinguely, Purusotam Basnet, Ganesh Acharya, Paramasivam Senthilkumaran, and Dalip Singh Mehta, *arXiv preprint arXiv:2002.07377* (2020).
- 6 N. Singla, V. Srivastava, and D. S. Mehta, *Journal of biophotonics* **11** (5), e201700279 (2018).
- 7 Hassaan Majeed, Shamira Sridharan, Mustafa Mir, Lihong Ma, Eunjung Min, Woongyu Jung, and Gabriel Popescu, *Journal of biophotonics* **10** (2), 177 (2017).
- 8 Barry R Masters, *Journal of Biomedical Optics* **17** (2), 029901 (2012).

- ⁹ YongKeun Park, Christian Depeursinge, and Gabriel Popescu, *Nature Photonics* **12** (10), 578 (2018).
- ¹⁰ P. Hariharan and Maitreyee Roy, *Journal of Modern Optics* **42** (11), 2357 (1995).
- ¹¹ Zili Lei, Xiaojun Liu, Li Zhao, Wenjun Yang, Cheng Chen, and Xiaoting Guo, *Journal of Microscopy* **276** (3), 118 (2019).
- ¹² Avner Safrani and Ibrahim Abdulhalim, *Opt. Lett.* **39** (2014).
- ¹³ Peter De Groot, (2011), pp. 167.
- ¹⁴ Mitsuo Takeda, Hideki Ina, and Seiji Kobayashi, *J. Opt. Soc. Am.* **72** (1), 156 (1982).
- ¹⁵ Natan T. Shaked, Yizheng Zhu, Matthew T. Rinehart, and Adam Wax, *Opt. Express* **17** (18), 15585 (2009).
- ¹⁶ Yasuhiro Awatsuji, Atsushi Fujii, Toshihiro Kubota, and Osamu Matoba, *Appl. Opt.* **45** (13), 2995 (2006).
- ¹⁷ Jun Woo Jeon and Ki-Nam Joo, *Sensors* **19** (23), 5094 (2019).
- ¹⁸ Vishal Srivastava, Mohammad Inam, Ranjeet Kumar, and Dalip Singh Mehta, *Journal of the Optical Society of Korea* **20** (6), 784 (2016).
- ¹⁹ Tatsuki Tahara, Yasuhiro Awatsuji, Yuki Shimosato, Takashi Kakue, Kenzo Nishio, Shogo Ura, Toshihiro Kubota, and Osamu Matoba, *Opt. Lett.* **36** (16), 3254 (2011).
- ²⁰ P Hariharan, BF Oreb, and Tomoaki Eiju, *Appl. Opt.* **26** (13), 2504 (1987).
- ²¹ Ian Goodfellow, Jean Pouget-Abadie, Mehdi Mirza, Bing Xu, David Warde-Farley, Sherjil Ozair, Aaron Courville, and Yoshua Bengio, presented at the Advances in neural information processing systems, 2014 (unpublished).
- ²² Deepak Pathak, Philipp Krahenbuhl, Jeff Donahue, Trevor Darrell, and Alexei A Efros, presented at the Proceedings of the IEEE conference on computer vision and pattern recognition, 2016 (unpublished).
- ²³ Jason Hu Weini Yu Zhouchangwan Yu.
- ²⁴ P. Isola, J. Zhu, T. Zhou, and A. A. Efros, presented at the 2017 IEEE Conference on Computer Vision and Pattern Recognition (CVPR), 2017 (unpublished).
- ²⁵ Azeem Ahmad, Vishesh Dubey, Ankit Butola, Jean-Claude Tinguely, Balpreet Singh Ahluwalia, and Dalip Singh Mehta, *Opt. Express* **28** (7), 9340 (2020).
- ²⁶ Z. Cheng and D. Liu, *Opt Lett* **44** (15), 3857 (2019).